International Journal of Nanomedicine

Dovepress
Taylor & Francis Group

Open Access Full Text Article

ORIGINAL RESEARCH

SYL3C Aptamer-DNA Tetrahedra Conjugates Enable Near-Infrared Fluorescent Imaging of Colorectal Cancer

Zhidie Huang[1], Pinghui Li[1], Yiwen Li[1], Xiaoyan Duan[2,3], Mengting Li[4,5], Dawei Jiang[4,5,*], Jianbo Li[2,3,*]

[1]Inner Mongolia Medical University, Hohhot, People's Republic of China; [2]Department of Nuclear Medicine, The Affiliated Hospital of Inner Mongolia Medical University, Hohhot, People's Republic of China; [3]Inner Mongolia Key Laboratory of Molecular Imaging, Hohhot, People's Republic of China; [4]Department of Nuclear Medicine, Union Hospital, Tongji Medical College, Huazhong University of Science and Technology, Wuhan, People's Republic of China; [5]Hubei Province Key Laboratory of Molecular Imaging, Wuhan, People's Republic of China

*These authors contributed equally to this work

Correspondence: Jianbo Li, The Affiliated Hospital of Inner Mongolia Medical University, 010050, Email lijianbo_1235@msn.cn, Dawei Jiang, Huazhong University of Science and Technology, 430022, Email daweijiang@hust.edu.cn

Purpose: SYL3C is an optimized DNA aptamer with high selectivity and affinity for the epithelial cell adhesion molecule (EpCAM), an overexpressed tumor antigen in colorectal cancer (CRC). While its cellular affinity has been validated, in vivo studies are lacking.

Methods: This study modifies SYL3C with the fluorescent motif Cy7 to evaluate its metabolism and diagnostic potential in EpCAM-positive HT-29 xenograft mice using near-infrared fluorescence (NIRF). We also employ DNA Tetrahedra (DTN) to load the Cy7-DTN-SYL3C probe and assess whether this strategy improves circulation and tumor uptake of SYL3C.

Results: Cy7-SYL3C is primarily metabolized by the kidneys and enables targeted imaging of HT-29 tumors, outperforming untargeted Cy7-DTN. The DTN coupling strategy prolongs SYL3C metabolism and enhances tumor probe uptake about twice higher than Cy7-SYL3C over 24 hours.

Conclusion: This study presents preliminary evidence for the SYL3C aptamer's potential in vivo imaging of EpCAM-positive CRC. The DTN conjugation strategy may extend the aptamer's metabolic stability and improve tumor uptake, expanding its applications in CRC diagnosis and treatment.

Keywords: epithelial cell adhesion molecule, aptamer, nanomaterial, molecular imaging, tumor

Graphical Abstract

Received: 7 December 2024
Accepted: 8 March 2025
Published: 19 March 2025

Introduction

Colorectal cancer (CRC) is a malignancy with about 50% of cases occurring at the rectum-sigmoid junction.[1] It is one of the top three cancers in terms of incidence and mortality rates worldwide, accounting for 10% of all cases.[2,3] Current imaging modalities for CRC have limitations, endoscopy may be unsuitable for the elderly or those with acute abdominal conditions such as peritonitis.[4] Computed tomography (CT) scans often miss small lesions.[5] Magnetic resonance imaging (MRI) struggles with small polyps and lymph nodes outside the pelvis, patients with implanted medical devices and uncooperative patients may be contraindicated for MRI procedures.[6] Transrectal ultrasound (TRU) accurately evaluates wall infiltration but is limited in lymph node assessment.[7] Thus, advanced imaging tools are needed. Molecular imaging is increasingly used for targeted imaging, patient stratification, drug selection, combination therapies, and immune modulation in CRC due to its non-invasive nature and targeted localization.[8–10] The key aspect is selecting therapeutic targets. Epithelial cell adhesion molecule (EpCAM) is a type I transmembrane glycoprotein, approximately 40 kDa in size,[11] that is overexpressed on the surface of CRC,[12] and the involvement in signal transduction,[13] migration,[14] proliferation,[15] and differentiation,[16] making it a promising target for monitoring and therapy in CRC.

Aptamers are single-stranded oligonucleotides with unique three-dimensional structures.[17] High selectivity and affinity, ease of preservation, shorter preparation timelines, reduced batch-to-batch variability making them effective probes in molecular imaging and treatment.[18–20] They are used in treating diseases like immune disorders, cardiovascular diseases, metabolic bone diseases, and various malignancies[21] that include CRC.[22,23] The SYL3C aptamer is an optimized DNA aptamer that targets the EpCAM site,[24] essential for detecting[25,26] and capturing[27,28] EpCAM-positive circulating tumor cells (CTCs) in heterogeneity,[29] stratification,[30] and therapeutic research.[31,32] For instance, Hu et al developed a non-enzymatic aptamer sensor that utilizes SYL3C to detect EpCAM expression across three breast cancer cell lines, potentially serving as an alternative to flow cytometry.[33] Additionally, Ren et al discovered a SYL3C-targeted delivery carrier designed to detect cancer cells and CTCs in peripheral blood.[26] Zhou et al leveraged the affinity of SYL3C for EpCAM-positive HT-29 cells to facilitate the controlled release of β-caryophyllene and paclitaxel (PTX) in response to pH changes.[34] However, in vivo imaging and metabolism studies of SYL3C in CRC are still lacking.

Aptamers are limited in clinical translation due to their short circulation time, requiring chemical modifications[17,35] like 2'-functional groups, phosphorothioate backbones, or PEG, which may cause allergic reactions.[36] A safer approach is to conjugate aptamers with carriers to increase molecular weight through nanostructural assembly, to exceed the renal filtration threshold,[37] enhancing circulation time. This requires controllable, biocompatible materials that maintain aptamer targeting efficacy. DNA tetrahedra (DTN) are ideal for aptamer conjugation due to their stability, favorable in vivo characteristics, extended half-life, and high bioavailability.[38,39] For example, Dai et al showed that MUC1-aptamer conjugated with DTN effectively delivered Doxorubicin,[40] while Zhan et al demonstrated enhanced specificity of the AS1411 aptamer with DTN.[41] Thus, we have selected the DTN conjugation strategy to improve the circulation and tumor uptake of the SYL3C aptamer, serving as a preliminary reference for SYL3C-targeted DTN-carrying drug therapy.

Fluorescent imaging probes for CRC span both clinical and experimental domains.[42,43] Clinically approved NIR-I tracers like indocyanine green (ICG) are routinely used for intraoperative guidance,[44] while experimental NIR-II probes targeting biomarkers such as CEACAM5[45] or CD24[46] aim to improve specificity. However, many probes face challenges[45,47,48] in stability, target-to-background ratio, or compatibility with cost-effective imaging systems. In this study, we selected Cy7 (Ex=750 nm, Em=773 nm), a chemically stable and low-toxicity NIR-I dye,[49] to label a SYL3C aptamer-nanoparticle conjugate, enabling straightforward validation of its targeting efficacy in HT-29 xenografts. This approach prioritizes mechanistic clarity over absolute imaging performance, providing a foundation for future optimization of fluorophore and targeting motifs.

This study modified the SYL3C aptamer with Cy7 to evaluate its metabolism and imaging potential in EpCAM-positive HT-29 xenograft mice using near-infrared fluorescence (NIRF). Results showed that Cy7-SYL3C was primarily metabolized by the kidneys and effectively targeted HT-29 tumors. The DTN conjugation strategy prolonged SYL3C's circulation time in tumor-bearing mice and nearly doubled tumor uptake, enhancing its imaging value. Fluorescence imaging revealed the metabolic distribution and tumor uptake of SYL3C in CRC mice, while further optimization of DTN provided valuable insights for CRC diagnosis and treatment. We developed a fluorescent tumor probe targeting

EpCAM, confirming its low biological toxicity and suitability for drug delivery therapy. The Cy7 performance also improved deep tissue imaging. We believe that ongoing optimization will enhance the probes' significance in CRC diagnosis and treatment, establishing a foundation for SYL3C's application in CRC.

Materials and Methods

General

DNA oligonucleotides (Cy5-SYL3C, Cy7-SYL3C, Azide-SYL3C) were obtained from Sangon Biotech (Shanghai,China). The McCoy's 5A (Modified) Medium and Dulbecco's Modified Eagle's Medium (DMEM) was purchased from GIBCO (Grand Island, NY, USA) and the Roswell Park Memorial Institute (RPMI) 1640 cell culture medium was purchased from Procell (Wuhan, China). The cell lines were purchased from Wuhan Sunncell Biotechnology Co., Ltd. (China) and sourced from various suppliers: Human Colorectal Adenocarcinoma Cell Line (HT-29, ATCC® CCL-185™) and Human Embryonic Kidney 293 Cell Line (HEK293, ATCC® CRL-1573™) from the American Type Culture Collection (ATCC), and Chinese Hamster Ovary Cell Line (CHO, ECACC No. 85051005) from the European Collection of Authenticated Cell Cultures (ECACC). Chemical reagents were obtained from Beijing Solarbio Science & Technology Co., Ltd. (China) and Demeter Biotechnology Co., Ltd. (China) and used as received, unless stated otherwise. The primary antibody and secondary antibodies for Western blotting were sourced from Proteintech Group Co., Ltd. (China). Enhanced Chemiluminescence Kit was purchased from Wuhan Boerfu Biotechnology Co., Ltd. (China).

Preparation and Purification of DTN-SYL3C

Four DNA oligonucleotide strands (sequences in Table S1) were annealed in TM buffer (10 mm Tris-base, 50 mm $MgCl_2$, pH 8.0) and rapidly cooled from 95°C to 4°C within 30 minutes to obtain DTN-DBCO. DTN-SYL3C was synthesized by reacting DTN-DBCO with Azide-SYL3C at room temperature (29°C) for 2 hours, followed by purification using 2% agarose gel electrophoresis at 4°C for 20 minutes, as validated in our previous work.[50]

Agarose Gel Electrophoresis

Agarose gel electrophoresis characterized the self-assembly of DTN-SYL3C. DNA samples were separated on a 2% agarose gel with a 1× TAE running buffer containing 12.5 mm $MgAc_2$ and run for 35 minutes at room temperature. Gels were imaged under imaging system (UVP GelStudio PLUS Touch, Germany).

Hydrodynamic Radius

The particle size of DTN-SYL3C was characterized using a Dynamic Light Scattering (DLS) instrument (Nano Series, Malvern Instruments). DTN and DTN-SYL3C solutions were prepared at 1.0 mL (50 μM) in phosphate buffer (pH 7.4). Suspensions were homogenized by filtration (0.22 μm syringe filter) prior to analysis. Measurements were conducted using a Malvern Zetasizer Nano ZS instrument at 25°C with three consecutive 5-minute runs. Key parameters included: average count rate = 500 kcps, polydispersity index (PDI) ≤ 0.08. Sample cuvettes were verified bubble-free before measurement.

Transmission Electron Microscope Observation of Morphology

TEM samples (DTN-SYL3C) were prepared by negative staining with 2% uranyl acetate (pH 4.5). Briefly, 5 μL aliquots were adsorbed onto carbon-coated copper grids (400 mesh) for 3 minutes, followed by staining for 2 minutes. Grids were air-dried overnight and imaged using a FEI TECNAI G2 20 TWIN microscope operated at 200 kV. Micrographs were acquired at 10,000× and 40,000× magnifications.

In vitro Stability

DTN-SYL3C was mixed with 100% mouse serum, fetal bovine serum (FBS), or 1× PBS buffer at a 1:10 ratio and incubated at 37°C for 24 hours. The stability was assessed using a 2% agarose gel with TAE-Mg^{2+} running buffer, and images were analyzed with ImageJ.

Cytotoxicity Assay

Cytotoxicity of DTN-SYL3C was evaluated using the Cell Counting Kit-8 (CCK-8). HT-29 cells were cultured in McCoy's 5A (Modified) Medium. HEK293 cells were cultured in DMEM and CHO cells were cultured in RPMI 1640 cell culture medium. All the aforementioned medium were supplemented with 10% FBS and 5% streptomycin/penicillin. Cells were incubated at 37°C with 5% CO_2. After seeding 5,000 cells per well in a 96-well plate and overnight culture, 10 μL of DTN-SYL3C at various concentrations of 25 nM, 50 nM, 100 nM, 250 nM, 500 nM, 1 μM was added to each well and incubated for 24 hours at 37°C. Then, 10 μL of CCK-8 solution was added and incubated at 37°C for 4 hours. Absorbance was measured at 450 nm using a microplate reader (Biotek Epoch, USA).

In vivo Safety Evaluation

Hematoxylin and eosin (H&E) staining of key organs was conducted to evaluate in vivo biosafety. DTN-SYL3C conjugates were administered intravenously at dose levels of 0.02 mg/kg (equivalent to 1 nM) in BALB/c healthy mice (6–7 weeks old), with an equal volume of PBS group as a control. After 24 hours, major organs (heart, liver, spleen, kidney, and lung) were collected, washed with PBS, fixed in 4% paraformaldehyde, and stored at 4°C for paraffin embedding and H&E staining, which were observed under a light microscope.

WB Validation of EpCAM Target Expression in HT-29 Cells

Tumor tissues and major organs (heart, liver, spleen, lung, and kidney) from HT-29 tumor-bearing mice were collected. Proteins were extracted and separated by SDS-PAGE (10% gel), then transferred to a 0.45 μm PVDF membrane. The membrane was blocked with 5% skimmed milk for 30 minutes, incubated overnight with a primary antibody at 4°C, and then with a secondary antibody for 30 minutes at room temperature. After washing, protein blots were detected using an Enhanced Chemiluminescence Kit, and band density was quantified with ImageJ software.

Immunofluorescence

Probe molecules for immunofluorescence experiments were labeled with Cy5 fluorescent dye due to fluorescence equipment requirements. Cy5-DTN and Cy5-DTN-DBCO were synthesized using a one-step annealing method that modified a DTN chain with Cy5. Cy5-DTN-SYL3C was prepared by purifying Cy5-DTN-DBCO with Azide-SYL3C. A Cy5-SYL3C solution was created by dissolving the dry powder in ultrapure water. The three fluorescent molecules were injected into HT-29 tumor-bearing BALB/c nude mice via the tail vein, and tumor tissues were collected 24 hours post-euthanasia. The tissues were fixed in 4% paraformaldehyde, dehydrated, and sectioned through paraffin embedding. The Goat Anti-Rabbit IgG H&L (Cy3, Ex: 550–554 nm, Em: 565–570 nm) dye (ab6939, Abcam, UK) was used for staining the EpCAM target. Fluorescent sections were observed under a fluorescence microscope (80i, Nikon, Japan), and images were captured. Results were assessed based on the blue color of the nucleus (DAPI staining), the red color of the target EpCAM, and the pink color of the injected fluorescent molecules under UV laser.

Construction of HT-29 Tumor-Bearing BALB/c Nude Mice

Female BALB/c Nude mice, aged 5–6 weeks, were sourced from Beijing Vital River Laboratory Animal Technology Co., Ltd. (China) and approved by the Ethics Committee of Inner Mongolia Medical University (approval number: YKD202402026). The study followed ethical guidelines and the Guide for the Care and Use of Laboratory Animals (National Research Council, 1996). Mice were housed in specific pathogen-free conditions with a 12-hour light cycle, temperature at 22 ± 2°C, and humidity at 44 ± 10%. IVC cages were regularly changed, and all materials were autoclaved. Mice were acclimatized for 5 days to 1 week post-purchase. For the HT-29 CRC subcutaneous tumor model, 1×10^6 HT-29 cells were injected into the right axilla. Tumors were used for in vivo imaging and biodistribution studies when they reached 8–10 mm in diameter.

Fluorescence Imaging

Cy7-DTN and Cy7-DTN-DBCO were synthesized using a one-step annealing method that modified a DTN chain with Cy7. Cy7-DTN-SYL3C was prepared by purifying Cy7-DTN-DBCO with Azide-SYL3C, as detailed in section 4.2. A solution of Cy7-SYL3C was created by dissolving the dry powder in ultrapure water. A total of 1 nM of Cy7-SYL3C, Cy7-DTN, and Cy7-DTN-SYL3C was injected into HT-29 tumor-bearing mice (n=3) via the tail vein, with anesthesia maintained using 2% isoflurane during imaging with a Lumina III optical system (PerkinElmer, USA). Camera temperature: −90°C. Mode: Fluorescent. Exposure: 1s. F/STOP:1. Binning: Medium; The field of view is 12.5 cm, and the subject height is 1.5 cm. The emission wavelength and excitation wavelength were Cy7 (Ex=750 nm, Em=773 nm). All mice were anesthetized in the RS83S Reward (Chinese anesthesia system) and imaged at the corresponding time points, all in the left lateral decubitus position with their heads upturned. Fluorescence imaging was performed at 1, 2, 4, 6, 8, 16, and 24 hours post-injection. After 24 hours, the mice were euthanized, and tumor tissue and major organs (heart, liver, spleen, lung, kidney) were excised for imaging. Regions of interest (ROIs) for the tumor and kidney were outlined for semi-quantitative analysis.

Statistical Analysis

Data were analyzed using GraphPad Prism 10.0, with quantitative results expressed as mean and standard deviation. One-way ANOVA compared group differences, with $p < 0.05$ deemed statistically significant.

Results

Preparation and Characterization of DTN-SYL3C

Four designed oligonucleotide single strands with reactive groups were combined in equal proportions and dissolved in TM annealing buffer. DTN-DBCO was synthesized through a one-step annealing procedure and reacted with Azide-SYL3C to yield DTN-SYL3C via click chemistry (Figure 1A). Sequence details of the oligonucleotides used for DTN-SYL3C assembly and the control group are in Table S1. The assembly process was monitored by agarose gel electrophoresis (Figure 1B). An increase in oligonucleotide strands led to a gradual increase in molecular weight, resulting in reduced migration speed within the gel over a consistent electrophoresis duration, with the position approaching the initial well until

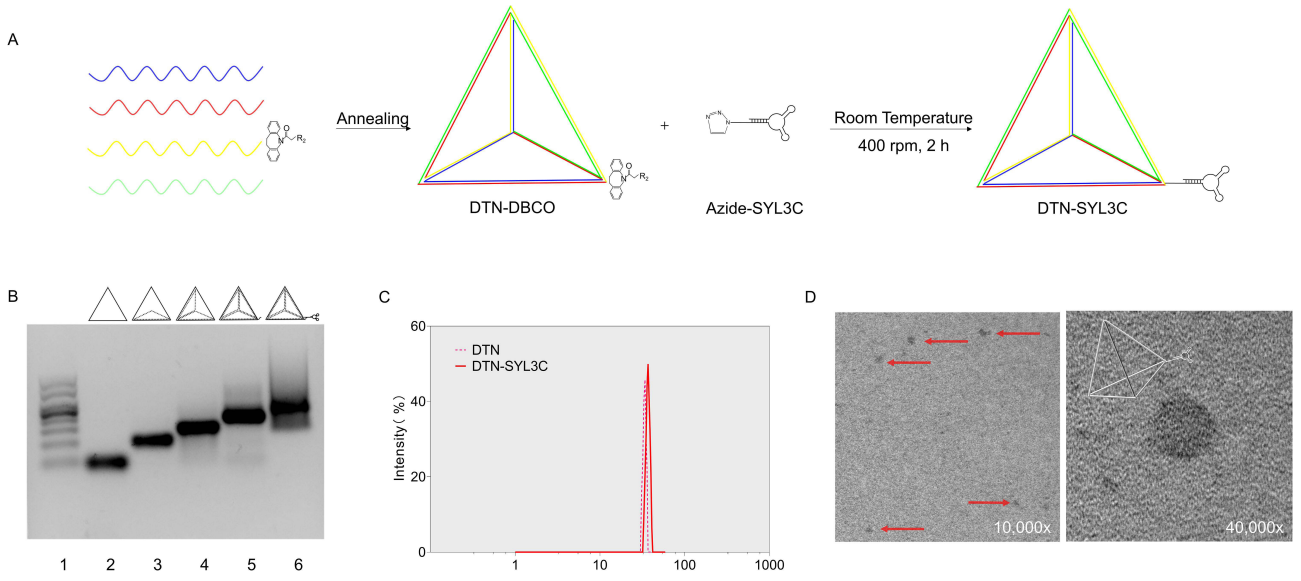

Figure 1 Illustrates the synthesis and characterization of DTN-SYL3C. (**A**) Schematic of the synthesis process. (**B**) Self-assembly analyzed via 2% agarose gel electrophoresis, with samples: 1: Marker; 2: S_1; 3: S_{1+2}; 4: S_{1+2+3}; 5: $S_{1+2+3+4}$ (DTN); 6: DTN-SYL3C. DNA samples were separated via 2% agarose gel using 1 × TAE buffer at 110 V for 40 minutes, followed by UV imaging (UVP GelStudio PLUS Touch, Germany). (**C**) Hydrated particle sizes of DTN and DTN-SYL3C were measured using dynamic light scattering (Nano Series, Malvern Instruments, UK), yielding sizes of approximately 15.82 ± 3.5 nm and 21.29 ± 2.2 nm, respectively. (**D**) Morphology of DTN-SYL3C particles was observed via transmission electron microscopy (TEM, USA), scale = 10,000×, 40,000×, respectively. The red arrows indicate the dispersed DTN-SYL3C particles.

https://doi.org/10.2147/IJN.S510964

DTN-SYL3C formation was achieved. Number 1–6 represent Marker, S_1, S_{1+2}, S_{1+2+3}, $S_{1+2+3+4}$ (DTN), and DTN-SYL3C, respectively. Dynamic light scattering (DLS) analysis showed that the average hydrodynamic diameters of DTN and DTN-SYL3C were 15.82 ± 3.5 nm and 21.29 ± 2.2 nm, respectively (Figure 1C). Transmission electron microscopy revealed the morphology of DTN-SYL3C (Figure 1D, scale = 10,000×, 40,000×, respectively).

In vitro Stability and Biosafety Assessment of DTN-SYL3C

DTN-SYL3C was subjected to co-culture with 1 × phosphate-buffered saline (PBS) buffer, 100% FBS, and 100% mouse serum over a specified duration to evaluate its in vitro stability. The findings indicated that approximately 80% of DTN-SYL3C retained its complete structural integrity for a minimum of 4 hours in both mouse and FBS (Figure 2A and B). The cytotoxicity of DTN-SYL3C was assessed using the CCK-8 assay. Following a 24-hour incubation of various concentrations of DTN-SYL3C with HT-29 cells, HEK 293 cells, and CHO cells, cell viability remained above 80% across all experimental conditions (Figure 2C). Histological examination through H&E staining revealed no significant differences between the DTN-SYL3C and PBS control groups, with no evident damage observed in major organ tissues (Figure 2D, scale bar = 50 μm). Collectively, these experiments substantiate that DTN-SYL3C is a biocompatible nanomaterial suitable for subsequent in vivo experimental investigations.

Verification of the Binding of DTN-SYL3C to the EpCAM Target

Tumor tissues were collected from HT-29 tumor-bearing nude mice, along with samples from the heart, liver, spleen, lung, and kidney, for Western blotting (WB) to confirm EpCAM expression on HT-29 cells (Figure 3A and B). GAPDH was used as the internal reference protein. Results indicated pronounced EpCAM expression on HT-29 tumors, minimal in the kidneys, and none in the heart, liver, spleen, or lung. Equal molar concentrations (1 nM) of Cy5-SYL3C, Cy5-DTN, and Cy5-DTN-SYL3C were administered via the tail vein. After 24 hours, the mice were euthanized, and tumor tissues were harvested (Figure 3C). Fluorescence microscopy showed that Cy5-SYL3C had a dispersed dot-like binding pattern, while Cy5-DTN had minimal binding. The Cy5-DTN-SYL3C group displayed significant binding to the EpCAM target in the red areas. Quantitative analysis using ImageJ (JACoB plugin) revealed Pearson's coefficients as follows:

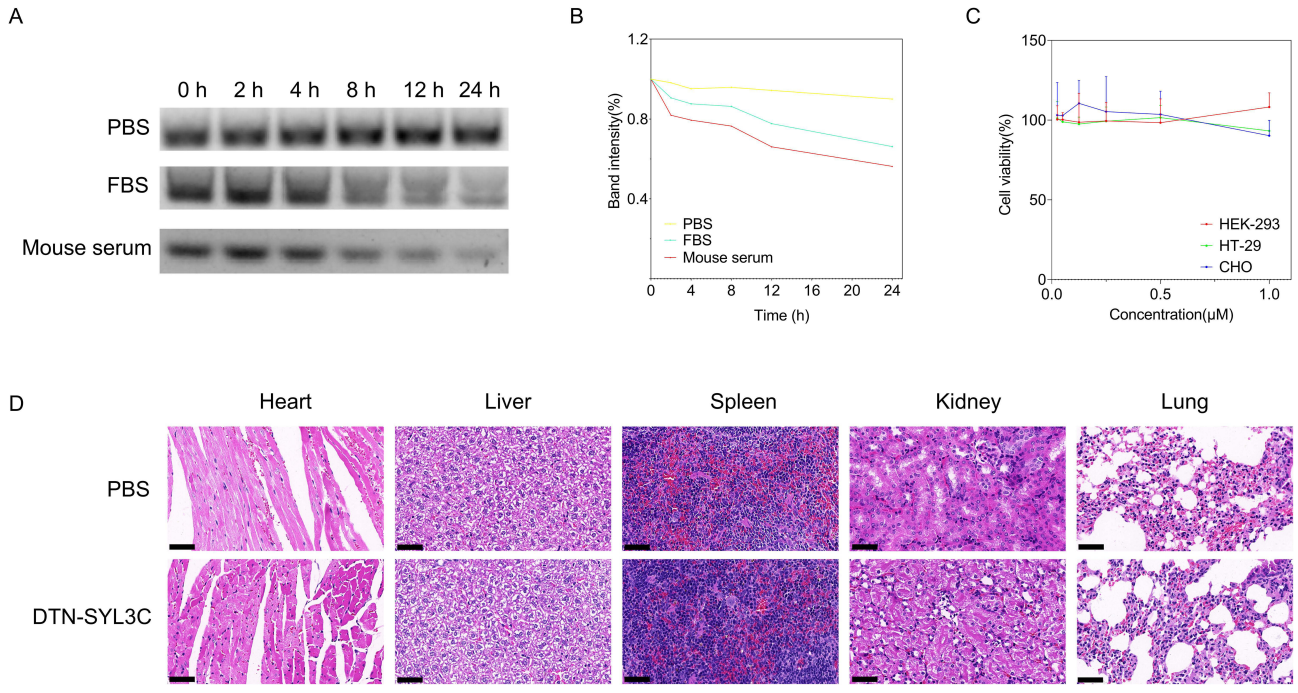

Figure 2 In vitro assessment of DTN-SYL3C stability and cytotoxicity. (**A**) Stability in PBS, FBS, and mouse serum was evaluated via 2% agarose gel electrophoresis. (**B**) Quantitative data from grayscale analysis in Figure 2A was obtained using ImageJ. (**C**) Cytotoxicity on HT-29, HEK293, and CHO cell lines was assessed with the CCK8 assay. (**D**) Histological sections of the heart, liver, spleen, kidney, and lung were collected 24 hours post-injection of DTN-SYL3C and PBS into healthy mice, scale bar = 50 μm.

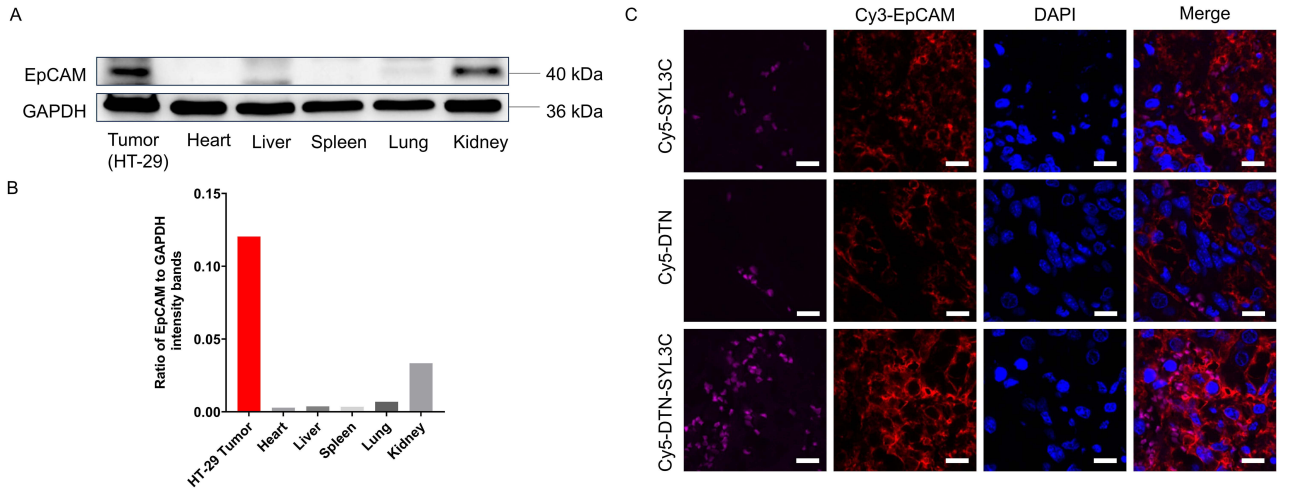

Figure 3 Illustrates the EpCAM expression in HT-29 tumors and validates the binding affinity of DTN-SYL3C to EpCAM. (**A**) Western blot results from tumor tissues and organs (heart, liver, spleen, lung, kidney) of HT-29 tumor-bearing mice identified EpCAM as the target protein, using a 10% SDS-PAGE gel and GAPDH as the internal reference. (**B**) Gray analysis of WB bands was conducted with ImageJ software to determine the ratio of the target protein's gray value to the internal reference. (**C**) Ex vivo immunofluorescence images were taken 24 hours after injecting Cy5-DTN, Cy5-SYL3C, and Cy5-DTN-SYL3C into HT-29 tumor-bearing mice. Scale bar = 10 μm. The Cy5 dye excitation wavelength 645–650 nm, emission wavelength 665–670 nm, labeled SYL3C, DTN, DTN-SYL3C, and appears as pink fluorescence. The Cy3 dye excites at 550–554 nm and emits at 565–570 nm and labels the target cell epithelial adhesion molecule (EpCAM) located on the surface of HT-29 cells, which fluoresces in red. DAPI excitation wavelength 330–380 nm, emission wavelength 420 nm, labels the nucleus, and appears as blue fluorescence. Merge means merging all images and displaying all tags. The model of the fluorescence microscope is 80i (Nikon, Japan), and the imaging system is FI3 (Nikon, Japan).

Cy5-SYL3C/Cy3-EpCAM was 0.32 ± 0.03, Cy5-DTN/Cy3-EpCAM was 0.18 ± 0.05, and Cy5-DTN-SYL3C/Cy3-EpCAM was 0.71 ± 0.08. These results suggest that the DTN conjugate strategy enhances SYL3C aptamer uptake in tumors while maintaining targeting capability. Scale bar = 10 μm.

Fluorescence Imaging

In vivo Fluorescence Imaging

Equal molar concentrations (1 nM) of Cy7-SYL3C, Cy7-DTN, and Cy7-DTN-SYL3C were administered via tail vein injection into HT-29 tumor-bearing mice (n=3). The mice were maintained under continuous anesthesia with 2% isoflurane, and in vivo fluorescence imaging was conducted at 1, 2, 4, 6, 8, 16, and 24 hours (Figure 4A). Fluorescence quantification was performed on both the kidneys and tumors at each imaging time point (Figures 4B) to further investigate the impact of the DTN conjugation strategy on the in vivo metabolism and tumor targeting of SYL3C. The results indicated that after administering Cy7-SYL3C, the fluorescence signal was predominantly localized in the liver and kidneys during the first four hours, shifting to a primary concentration in the kidneys thereafter. The fluorescence intensity in the kidneys subsequently decreased, suggesting that the SYL3C aptamer is primarily metabolized by the renal system. The lower molecular weight of Cy7-SYL3C facilitates a more rapid metabolic process than the non-targeting Cy7-DTN, resulting in an overall reduction in fluorescence signals observed in the kidneys. Conversely, Cy7-SYL3C exhibited enhanced and prolonged fluorescence signals at the tumor site. Coupled with immunofluorescence experiments, these results indicate that the accumulation of the SYL3C aptamer at the tumor site is primarily due to its specific binding to the EpCAM target, confirming the aptamer's capability for targeted imaging in EpCAM-positive HT-29 CRC models. Following conjugation with DTN, the fluorescence signal of Cy7-DTN-SYL3 exhibited predominant localization in the liver and kidneys. Notably, the fluorescence intensity in the kidneys increased by an average of 1.8 to 2 times higher from 2 to 24 hours compared to Cy7-SYL3C, which was statistically significant. This observation suggests that DTN conjugation has effectively prolonged the in vivo circulation time of SYL3C to a certain degree. Tumor fluorescence intensity data revealed that Cy7-DTN-SYL3C retained in the tumor for at least 8 hours longer than non-targeting Cy7-DTN, demonstrating the aptamer's targeting effect. Additionally, Cy7-DTN-SYL3C exhibited higher fluorescence intensity with tumor uptake is about twice higher than Cy7-SYL3C over 24 hours, indicating superior imaging efficacy for CRC. In vivo imaging confirmed that the DTN coupling strategy improved SYL3C's stability and targeted uptake in tumors.

https://doi.org/10.2147/IJN.S510964

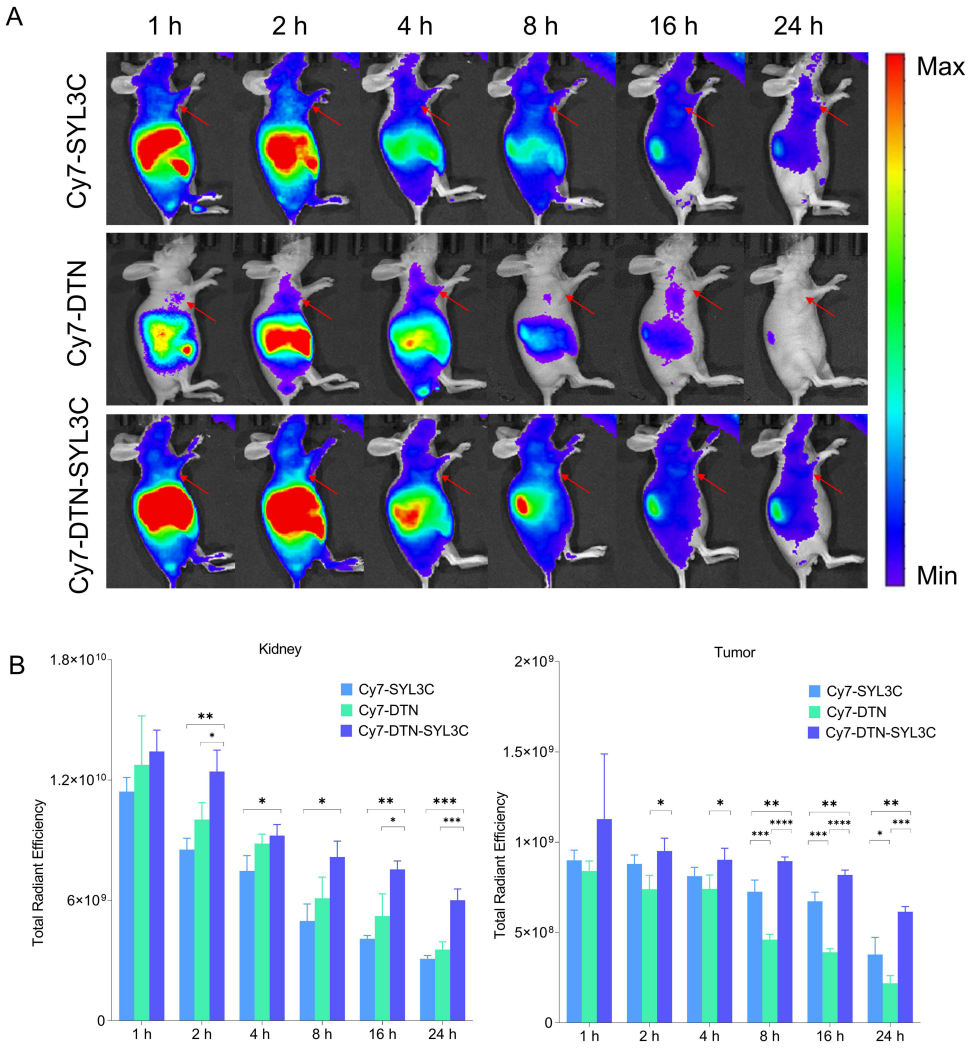

Figure 4 In vivo Fluorescence Imaging. (**A**) Cy7-SYL3C, Cy7-DTN, and Cy7-DTN-SYL3C was conducted in HT-29 tumor-bearing mice at various time points, with red arrows indicating tumor locations. (**B**) Fluorescence counts in the kidneys and tumors were compared at different time points in vivo (n=3, *P < 0.05, **P < 0.01, ***P < 0.001, ****P < 0.0001).

Ex vivo Organ Fluorescence Imaging

Mice were euthanized and dissected 24 hours post-in vivo imaging, and abdominal wall tissue was removed to minimize intestinal gas interference. Tumor tissues and major organs, including the heart, liver, spleen, lungs, and kidneys, were excised and imaged (Figure 5A). A semi-quantitative analysis was conducted on the kidneys and tumors, with fluorescence counts recorded (Figure 5B). The results indicated that the uptake of Cy7-DTN-SYL3C in both the kidneys and tumors at the 24-hour mark was maximal. See Figure S1 for a comparison of fluorescence counts of other related organs of interest. It can be seen that after conjugation, the metabolic organs of Cy7-DTN-SYL3C include not only the kidney, but also the liver. Notably, despite the significant molecular weight difference between DTN and the aptamer, the uptake of Cy7-SYL3C in the tumor exceeded that of Cy7-DTN, demonstrating the active targeting capability of SYL3C. Additionally, while the molecular weight disparity between the Cy7-DTN-SYL3C conjugate and Cy7-DTN was not significant, the fluorescence counts for the Cy7-DTN-SYL3C conjugate in the kidneys and tumors were markedly higher than those for Cy7-DTN. This observation suggests that the aptamer-mediated targeting modification enhanced the in vivo retention time of Cy7-DTN-SYL3C and improved targeted tumor uptake. Furthermore, the fluorescence counts of the Cy7-DTN-SYL3C conjugate in tumors exceeded those of the Cy7-SYL3C, reinforcing the notion that the DTN conjugation strategy offers are superior imaging tool for CRC.

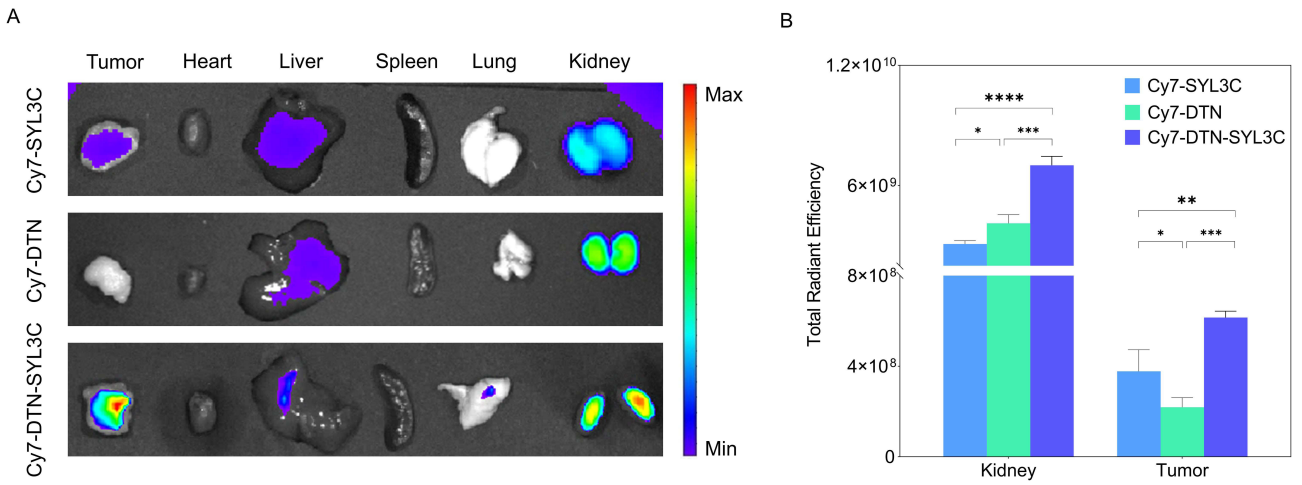

Figure 5 Ex vivo Organ Fluorescence Imaging. (**A**) Ex vivo imaging of organs was performed 24 hours post-injection of the different probes. (**B**) Fluorescence counts in the kidneys and tumors were assessed for the different probe groups after a 24-hour period ex vivo (n=3, *P < 0.05, **P < 0.01, ***P < 0.001, ****P < 0.0001).

Discussion

Aptamers, as molecular probes with high specificity and engineering flexibility, exhibit superior tumor penetration and lower immunogenicity compared to antibodies, positioning them as promising agents for tumor theranostics. In this study, we developed a DTN-conjugated SYL3C aptamer system targeting EpCAM, a pan-carcinoma antigen over-expressed in CRC. There are three key innovations distinguish our work: (1) The rational integration of DTN nanocarriers prolonged the aptamer's plasma half-life to ~24 hours (about 2-fold longer than free SYL3C), indirectly enhancing tumor accumulation as evidenced by sustained fluorescence signals; (2) In vivo validation revealed SYL3C's renal-dominated clearance pathway and specific HT-29 tumor targeting, contrasting with non-targeted tetrahedral nanostructures of larger size; (3) We demonstrated the dual functionality of DTN-SYL3C as both an imaging probe and a potential drug delivery platform, addressing the critical need for tumor-selective theranostic systems. While this strategy mitigates aptamers' inherent limitation of rapid clearance, challenges persist: The modest fluorescence enhancement warrants optimization of dosing regimens, and hepatic metabolism of conjugates requires rigorous safety assessment before clinical translation. Conjugation with DTN increased tumor fluorescence intensity from 3.1×10^8 (SYL3C alone) to 5.9×10^8 ($p<0.01$), achieving a tumor-to-background ratio (TBR) of 3.05 versus 1.08 for the non-conjugated probe (DTN alone). While the sensitivity of Cy7-SYL3C-DTN compared to clinical-grade anti-EpCAM antibody probes needs optimization, our platform provides key advantages in modularity and synthetic scalability for future theranostic applications. Future studies should prioritize three directions: (1) Quantitative PET imaging to map EpCAM expression heterogeneity across tumor types (eg, breast/lung cancers); (2) Multimodal imaging integration (eg, MRI/CT-compatible probes) for anatomical-functional correlation; (3) Structure-activity optimization of DTN-aptamer interfaces to balance circulation time and tumor penetration. Collectively, this work establishes a framework for engineering aptamer-based theranostic platforms to promote the diagnosis of CRC.

Conclusion

This study confirmed that the combination of DTN and SYL3C aptamer can effectively prolong the in vivo metabolism time of aptamers, and confirmed that DTN has specific targeting ability for HT-29 xenograft tumors by increasing the tumor fluorescence intensity, which provides an experimental basis for EpCAM-positive tumor molecular imaging. Although aptamers still face clinical translation bottlenecks such as short in vivo half-lives and potential toxicity, the clinical application of aptamers in the integration of cancer diagnosis and treatment will be promoted by optimizing the delivery system (eg, using PET quantitative analysis) and developing a multimodal imaging strategy (combined with MRI/CT).

https://doi.org/10.2147/IJN.S510964

Abbreviations

EpCAM, epithelial cell adhesion molecule, CRC, colorectal cancer, NIRF, near-infrared fluorescence, DTN, DNA Tetrahedra, CT, Computed tomography, MRI, Magnetic resonance imaging, TRU, Transrectal ultrasound, CTCs, circulating tumor cells (CTCs), PTX, paclitaxel, DMEM, Dulbecco's Modified Eagle's Medium, RPMI, Roswell Park Memorial Institute.

Institutional Review Board Statement

The animal study protocol was adhered to ethical standards and was approved by the Ethics Committee of Inner Mongolia Medical University (approval number: YKD202402026).

Data Sharing Statement

The original contributions presented in the study are included in the article/Supplementary Material, further inquiries can be directed to the corresponding authors.

Acknowledgment

We thank our teammates Hao Wang, Li Wen, and Chengwen Zheng for their collaboration and support in writing this paper.

Author Contributions

All authors made a significant contribution to the work reported, whether that is in the conception, study design, execution, acquisition of data, analysis and interpretation, or in all these areas; took part in drafting, revising or critically reviewing the article; gave final approval of the version to be published; have agreed on the journal to which the article has been submitted; and agree to be accountable for all aspects of the work. All authors have read and agreed to the published version of the manuscript.

Funding

This work is supported by the National Natural Science Foundation of China (82060324), "Youth Science and Technology Talents in Colleges and Universities" Support Program Project of Inner Mongolia Education Department (NJYT22016), the Natural Science Foundation of lnner Mongolia Autonomous Region (2024MS08075), the National Key Research and Development Program of China (2022YFB3808200), the National Natural Science Foundation of China (22277031), and Hubei Science and Technology Innovation Talent Program (2023DJC162).

Disclosure

The authors have no conflicts of interest to declare for this work.

References

1. Lauby-Secretan B, Vilahur N, Bianchini F, Guha N, Straif K. The IARC perspective on colorectal cancer screening. *N Engl J Med*. 2018;378(18):1734–1740. doi:10.1056/NEJMsr1714643
2. Siegel RL, Miller KD, Wagle NS, Jemal A. Cancer statistics, 2023. *CA Cancer J Clin*. 2023;73(1):17–48. doi:10.3322/caac.21763
3. Amintas S, Dupin C, Boutin J, et al. Bioactive food components for colorectal cancer prevention and treatment: a good match. *Crit Rev Food Sci Nutr*. 2023;63(23):6615–6629. doi:10.1080/10408398.2022.2036095
4. Nguyen VX, Nguyen VTL, Nguyen CC. Appropriate use of endoscopy in the diagnosis and treatment of gastrointestinal diseases: up-to-date indications for primary care providers. *Int J Gen Med*. 2010;3:345–357. doi:10.2147/ijgm.S14555
5. De Haan MC, Pickhardt PJ, Stoker J. CT colonography: accuracy, acceptance, safety and position in organised population screening. *Gut*. 2015;64(2):342–350. doi:10.1136/gutjnl-2014-308696
6. Sobeh T, Inbar Y, Apter S, et al. Diffusion-weighted MRI for predicting and assessing treatment response of liver metastases from CRC – a systematic review and meta-analysis. *Eur J Radiol*. 2023;163:110810. doi:10.1016/j.ejrad.2023.110810
7. Lotfollahzadeh S, Kashyap S, Tsoris A, Recio-Boiles A, Babiker HM. *Rectal Cancer. StatPearls*. StatPearls P Copyright ©; 2024.
8. Rodríguez-Fraile M, Cózar-Santiago MP, Sabaté-Llobera A, et al. FDG PET/CT in colorectal cancer. *Rev Esp Med Nucl Imagen Mol*. 2020;39(1):57–66. doi:10.1016/j.remn.2019.09.009
9. Xu D, Lu X, Yang F, et al. STING-targeted PET tracer for early assessment of tumor immunogenicity in colorectal cancer after chemotherapy. *Eur J Nucl Med Mol Imaging*. 2024;51(3):641–655. doi:10.1007/s00259-023-06485-w
10. Li K, Liu W, Yu H, et al. 68Ga-FAPI PET imaging monitors response to combined TGF-βR inhibition and immunotherapy in metastatic colorectal cancer. *J Clin Invest*. 2024;134(4). doi:10.1172/jci170490

11. Litvinov SV, Velders MP, Bakker HA, Fleuren GJ, Warnaar SO. Ep-CAM: a human epithelial antigen is a homophilic cell-cell adhesion molecule. *J Cell Biol*. 1994;125(2):437–446. doi:10.1083/jcb.125.2.437
12. Herlyn M, Steplewski Z, Herlyn D, Koprowski H. Colorectal carcinoma-specific antigen: detection by means of monoclonal antibodies. *Proc Natl Acad Sci U S A*. 1979;76(3):1438–1442. doi:10.1073/pnas.76.3.1438
13. Moustafa M, Dähling KK, Günther A, et al. Combined Targeting of AKT and mTOR inhibits tumor formation of EpCAM(+) and CD90(+) human hepatocellular carcinoma cells in an orthotopic mouse model. *Cancers*. 2022. 148. doi:10.3390/cancers14081882
14. Fagotto F, Aslemarz A. EpCAM cellular functions in adhesion and migration, and potential impact on invasion: a critical review. *Biochim Biophys Acta Rev Cancer*. 2020;1874(2):188436. doi:10.1016/j.bbcan.2020.188436
15. Gires O, Pan M, Schinke H, Canis M, Baeuerle PA. Expression and function of epithelial cell adhesion molecule EpCAM: where are we after 40 years? *Cancer Metastasis Rev*. 2020;39(3):969–987. doi:10.1007/s10555-020-09898-3
16. Kalantari E, Taheri T, Fata S, et al. Significant co-expression of putative cancer stem cell markers, EpCAM and CD166, correlates with tumor stage and invasive behavior in colorectal cancer. *World J Surg Oncol*. 2022;20(1):15. doi:10.1186/s12957-021-02469-y
17. Zhu G, Chen X. Aptamer-based targeted therapy. *Adv Drug Deliv Rev*. 2018;134:65–78. doi:10.1016/j.addr.2018.08.005
18. Arévalo AP, Castelli R, Ibarra M, Crispo M, Calzada V. In vivo evaluation of Sgc8-c aptamer as a molecular imaging probe for colon cancer in a mouse xenograft model. *Int J mol Sci*. 2022;23(5):2466. doi:10.3390/ijms23052466
19. Li Y, Li T, Chen H, et al. Engineering AND-gate aptamer-signal base conjugates for targeted magnetic resonance molecular imaging of metastatic cancer. *ACS Appl Mater Interfaces*. 2022;14(15):17032–17041. doi:10.1021/acsami.1c24048
20. Song W, Song Y, Li Q, Fan C, Lan X, Jiang D. Advances in aptamer-based nuclear imaging. *Eur J Nucl Med Mol Imaging*. 2022;49(8):2544–2559. doi:10.1007/s00259-022-05782-0
21. Nimjee SM, White RR, Becker RC, Sullenger BA. Aptamers as Therapeutics. *Annu Rev Pharmacol Toxicol*. 2017;57:61–79. doi:10.1146/annurev-pharmtox-010716-104558
22. Cha BS, Jang YJ, Lee ES, et al. Development of a Novel DNA aptamer targeting colorectal cancer cell-derived small extracellular vesicles as a potential diagnostic and therapeutic agent. *Adv Healthc Mater*. 2023;12(27):e2300854. doi:10.1002/adhm.202300854
23. Niu B, Wu Y, Zhou M, et al. Precise delivery of celastrol by PEGylated aptamer dendrimer nanoconjugates for enormous therapeutic effect via superior intratumor penetration over antibody counterparts. *Cancer Lett*. 2023;579:216461. doi:10.1016/j.canlet.2023.216461
24. Song Y, Zhu Z, An Y, et al. Selection of DNA aptamers against epithelial cell adhesion molecule for cancer cell imaging and circulating tumor cell capture. *Anal Chem*. 2013;85(8):4141–4149. doi:10.1021/ac400366b
25. Han D, Ren XH, Liao XR, et al. A multiple targeting nanoprobe for identifying cancer metastatic sites based on detection of various mRNAs in circulating tumor cells. *Nano Lett*. 2023;23(9):3678–3686. doi:10.1021/acs.nanolett.2c04643
26. Ren XH, Han D, He XY, et al. Multi-targeting nano-systems targeting heterogeneous cancer cells for therapeutics and biomarker detection. *Adv Healthc Mater*. 2023;12(4):e2202155. doi:10.1002/adhm.202202155
27. Gao T, Ding P, Li W, Wang Z, Lin Q, Pei R. Isolation of DNA aptamers targeting N-cadherin and high-efficiency capture of circulating tumor cells by using dual aptamers. *Nanoscale*. 2020;12(44):22574–22585. doi:10.1039/d0nr06180h
28. Xiao Y, Zhou Z, Zuo Y, et al. Layer-by-layer fabrication of alginate/polyethyleneimine multilayer on magnetic interface with enhanced efficiency in immuno-capturing circulating tumor cells. *Anal Chim Acta*. 2024;1312:342778. doi:10.1016/j.aca.2024.342778
29. Liu X, Zhang W, Gu J, Wang J, Wang Y, Xu Z. Single-cell SERS imaging of dual cell membrane receptors expression influenced by extracellular matrix stiffness. *J Colloid Interface Sci*. 2024;668:335–342. doi:10.1016/j.jcis.2024.04.170
30. Wang Y, Jie H, Ye H, Zhang Y, Li N, Zhuang J. Methylene blue-stained single-stranded DNA aptamers as a highly efficient electronic switch for quasi-reagentless exosomes detection: an old dog with new tricks. *Anal Chem*. 2023;95(49):18166–18173. doi:10.1021/acs.analchem.3c03715
31. Mashreghi M, Zamani P, Moosavian SA, Jaafari MR. Anti-epcam aptamer (Syl3c)-functionalized liposome for targeted delivery of doxorubicin in vitro and in vivo antitumor studies in mice bearing c26 colon carcinoma. *Nanoscale Res Lett*. 2020;15(1):101. doi:10.1186/s11671-020-03334-9
32. Yavari B, Athari SS, Omidi Y, Jalali A, Najafi R. EpCAM aptamer activated 5-FU-loaded PLGA nanoparticles in CRC treatment; in vitro and in vivo study. *J Drug Target*. 2023;31(3):296–309. doi:10.1080/1061186x.2022.2148679
33. Hu Z, Yang Z, Chen M, et al. Double hook-type aptamer-based colorimetric and electrochemical biosensor enables rapid and robust analysis of EpCAM expression. *Biosens Bioelectron*. 2024;266:116717. doi:10.1016/j.bios.2024.116717
34. Zhou X, Cao C, Li N, Yuan S. SYL3C aptamer-anchored microemulsion co-loading β-elemene and PTX enhances the treatment of colorectal cancer. *Drug Deliv*. 2019;26(1):886–897. doi:10.1080/10717544.2019.1660733
35. Meek KN, Rangel AE, Heemstra JM. Enhancing aptamer function and stability via in vitro selection using modified nucleic acids. *Methods*. 2016;106:29–36. doi:10.1016/j.ymeth.2016.03.008
36. Kozma GT, Shimizu T, Ishida T, Szebeni J. Anti-PEG antibodies: properties, formation, testing and role in adverse immune reactions to PEGylated nano-biopharmaceuticals. *Adv Drug Deliv Rev*. 2020;154-155:163–175. doi:10.1016/j.addr.2020.07.024
37. Ding D, Yang C, Lv C, Li J, Tan W. Improving Tumor Accumulation of Aptamers by Prolonged Blood Circulation. *Anal Chem*. 92(5):4108–4114. doi:10.1021/acs.analchem.9b05878
38. Tian T, Zhang T, Shi S, Gao Y, Cai X, Lin Y. A dynamic DNA tetrahedron framework for active targeting. *Nat Protoc*. 2023;18(4):1028–1055. doi:10.1038/s41596-022-00791-7
39. Xie N, Liu S, Yang X, He X, Huang J, Wang K. DNA tetrahedron nanostructures for biological applications: biosensors and drug delivery. *Analyst*. 2017;142(18):3322–3332. doi:10.1039/c7an01154g
40. Dai B, Hu Y, Duan J, Yang XD. Aptamer-guided DNA tetrahedron as a novel targeted drug delivery system for MUC1-expressing breast cancer cells in vitro. *Oncotarget*. 2016;7(25):38257–38269. doi:10.18632/oncotarget.9431
41. Zhan Y, Ma W, Zhang Y, et al. DNA-based nanomedicine with targeting and enhancement of therapeutic efficacy of breast cancer cells. *ACS Appl Mater Interfaces*. 2019;11(17):15354–15365. doi:10.1021/acsami.9b03449
42. Kim SY, Kim J, Kim H, et al. Fluorescence-guided tumor visualization of colorectal cancer using tumor-initiating probe yellow in preclinical models. *Sci Rep*. 2024;14(1):26946. doi:10.1038/s41598-024-76312-1
43. Lwin TM, Turner MA, Amirfakhri S, Nishino H, Hoffman RM, Bouvet M. Fluorescence molecular targeting of colon cancer to visualize the invisible. *Cells*. 2022;11(2):249. doi:10.3390/cells11020249

44. Cassinotti E, Boni L, Baldari L. Application of indocyanine green (ICG)-guided surgery in clinical practice: lesson to learn from other organs-an overview on clinical applications and future perspectives. *Updates Surg*. 2023;75(2):357–365. doi:10.1007/s13304-022-01361-y
45. Guo X, Li C, Jia X, et al. NIR-II fluorescence imaging-guided colorectal cancer surgery targeting CEACAM5 by a nanobody. *EBioMedicine*. 2023;89:100476. doi:10.1016/j.ebiom.2023.104476
46. Guo X, Luo S, Wang X, et al. CD24-targeted NIR-II fluorescence imaging enables early detection of colorectal neoplasia. *Cancer Res*. 2024;84 (23):4099–4113. doi:10.1158/0008-5472.Can-24-0012
47. Fang J, Lin L, Tan J, et al. Targeting the CD24-siglec10 axis: a potential strategy for cancer immunotherapy. *BIO Integration*. 2024;5(1):997. doi:10.15212/bioi-2023-0022
48. Zhao K, Wu C, Li X, et al. From mechanism to therapy: the journey of CD24 in cancer. *Front Immunol*. 2024;15:1401528. doi:10.3389/fimmu.2024.1401528
49. Pagano JM, Clingman CC, Ryder SP. Quantitative approaches to monitor protein-nucleic acid interactions using fluorescent probes. *Rna*. 2011;17 (1):14–20. doi:10.1261/rna.2428111
50. Li P, Huang Z, Duan X, et al. PET image-guided kidney injury theranostics enabled by a bipyramidal DNA framework. Biomater. Sci. 2024;12 (8):2086–2095. doi:10.1039/d3bm01575k